136 (2022) 212782

Contents lists available at ScienceDirect

Biomaterials Advances

journal homepage: www.journals.elsevier.com/materials-science-and-engineering-c

Biophysical properties of hydrogels for mimicking tumor extracellular matrix

Anna P. Cameron [a], Bijun Zeng [b], Yun Liu [a], Haofei Wang [a], Farhad Soheilmoghaddam [a], Justin Cooper-White [a,c], Chun-Xia Zhao [a,*]

[a] *Australian Institute of Bioengineering and Nanotechnology, The University of Queensland, St Lucia, QLD 4072, Australia*
[b] *Diamantina Institute, The University of Queensland, St Lucia, QLD 4072, Australia*
[c] *School of Chemical Engineering, The University of Queensland, Brisbane, QLD 4072, Australia*

ARTICLE INFO

Keywords:
Cancer
Hydrogel
Extracellular matrix
Biophysical properties
Complex modulus
Loss tangent

ABSTRACT

The extracellular matrix (ECM) is an essential component of the tumor microenvironment. It plays a critical role in regulating cell-cell and cell-matrix interactions. However, there is lack of systematic and comparative studies on different widely-used ECM mimicking hydrogels and their properties, making the selection of suitable hydrogels for mimicking different *in vivo* conditions quite random. This study systematically evaluates the biophysical attributes of three widely used natural hydrogels (Matrigel, collagen gel and agarose gel) including complex modulus, loss tangent, diffusive permeability and pore size. A new and facile method was developed combining Critical Point Drying, Scanning Electron Microscopy imaging and a MATLAB image processing program (CSM method) for the characterization of hydrogel microstructures. This CSM method allows accurate measurement of the hydrogel pore size down to nanometer resolution. Furthermore, a microfluidic device was implemented to measure the hydrogel permeability (P_d) as a function of particle size and gel concentration. Among the three gels, collagen gel has the lowest complex modulus, medium pore size, and the highest loss tangent. Agarose gel exhibits the highest complex modulus, the lowest loss tangent and the smallest pore size. Collagen gel and Matrigel produced complex moduli close to that estimated for cancer ECM. The P_d of these hydrogels decreases significantly with the increase of particle size. By assessing different hydrogels' biophysical characteristics, this study provides valuable insights for tailoring their properties for various three-dimensional cancer models.

1. Introduction

The tumor microenvironment (TME) plays a substantial role in each phase of the tumor progression, including cancer cell proliferation, invasion, and metastasis [1]. The extracellular matrix (ECM) from which the tumor is composed has attracted increasing attention in recent years, being recognized as an essential factor for studying the TME *in vitro* and creating pathophysiologically-relevant disease models. The ECM is composed of a complex, heterogeneous mixture of proteins, proteoglycans, glycoproteins and other accessory molecules. The structure of the ECM provides spatial and mechanical support for cells in the TME, including immune cells, fibroblasts and endothelial cells [2]. In addition to its role as the structural support, the ECM is also responsible for informing and regulating the function and phenotype of these cells [3]. It acts physically as a molecular barrier between epithelial cells and other connective tissue cells, while permitting the diffusion of gas and transport of molecules to cells through the TME.

The cancer cell-ECM relationship is multidimensional, but an important aspect of this exchange occurs during tumor growth and metastasis. During metastasis, cancer interacts with the ECM through soluble signals, resulting in the transition of cells into a more invasive (mesenchymal) phenotype [3]. With the assistance of the ECM, these cells migrate into surrounding connective tissue (stroma) [3]. ECM is also involved when polarized epithelial cells assume a mesenchymal phenotype, which in turn greatly stimulate the production of different ECM components, remodeling the ECM [2]. A remodeled ECM demonstrates changes in its biophysical characteristics, which have been linked to increased tumor invasiveness and metastatic potential [2,4]. For example, stiffness changes and abnormal ECM deposition are often observed [5].

---

* Corresponding author.
E-mail address: z.chunxia@uq.edu.au (C.-X. Zhao).

https://doi.org/10.1016/j.bioadv.2022.212782
Received 4 November 2021; Received in revised form 1 March 2022; Accepted 26 March 2022
Available online 30 March 2022
2772-9508/© 2022 Elsevier B.V. All rights reserved.

The biophysical properties of the ECM in the tumor microenvironment play a critical role in cancer progression including stiffness, porosity, spatial arrangement and orientation [1]. The systematic study of these properties provides important information for establishing reliable and relevant *in vitro* tumor models that mimic *in vivo* conditions. Compared to traditional two-dimensional models, three-dimensional (3D) tumor models incorporating the ECM have been demonstrated to be more clinically relevant and are becoming the standard for establishing disease models [6].

3D tumor models utilize hydrogel scaffolds as an ECM substitute [7]. Hydrogels produce a porous structure to mimic the native ECM [7,8]. These matrices can be either biologically derived or synthetic in origin, though biologically derived (natural) hydrogels are considered the gold standard. Matrigel, collagen and agarose are the three most widely used naturally occurring hydrogels. Matrigel, the most commonly used hydrogel, is the reconstituted ECM of an Engelbreth-Holm-Swarm mouse sarcoma [9]. Collagen gel, made from type I collagen and known to be critical to cancer progression, is commonly isolated from a rat tail [9]. Agarose gel, a polysaccharide polymer derived from seaweed, is commonly used in biological assays, though it lacks cell adhesion moieties that are critical for long-term adherent cell culture [10,11]. Agarose is still heavily implemented in tumor models as a cell barrier [12–15], a method of gauging compressive stress around spheroids [16] and in the production of tumor spheroids [12,14]. Also, agarose gel is often used in combination with Matrigel or collagen gel to utilize its higher complex modulus to mimic stiffer ECM mimicking hydrogels [17–19]. These hydrogels offer a biocompatible scaffold with adjustable biophysical properties, including pore-size, diffusive permeability, complex modulus (a stiffness approximation) and viscoelasticity (Fig. 1).

As these hydrogels are of biological origin, it is difficult to standardize their physical properties, and therefore their isolated impact on the establishment of tumor models. To create a more pathophysiologically-relevant ECM, the biophysical aspects (complex modulus, viscoelasticity, pore size, and diffusive permeability) of these hydrogels need to be characterized, with their interdependence understood, so as to be tailored to accommodate each tumor type [1]. This study will provide valuable information for engineering different hydrogels for mimicking ECM in the tumor microenvironment (Fig. 1).

2. Experimental details

2.1. Materials

Skov3 cells, a human ovarian cancer cell line with epithelial-like morphology, were purchased from the American Type Culture Collection. Skov3 cells were cultured in high-glucose Dulbecco's modified. Dulbecco's modified Eagle's medium (DMEM), trypsin, fetal bovine serum (FBS), Penicillin-Streptomycin were purchased from GIBCO (USA). Water was obtained from a Milli-Q system (Millipore, North Ryde, Australia) equipped with a 0.22 μm filter and had resistivity larger than 18.2 MΩ cm. Corning® Matrigel® matrix and Corning® Collagen I, High Concentration Rat Tail (9.43 mg/mL) were purchased from Corning Incorporated (New York, USA). Low melting point agarose, agarose, phosphate buffer saline (PBS) tablets, sodium hydroxide (NaOH) (1.0 M), ethyl alcohol (ethanol), chloroform and anhydrous isopropyl alcohol (IPA) were purchased from Sigma-Aldrich (St. Louis, MO, USA). Sylgard 184 Silicone Elastomer curing agent, Sylgard 184 Silicone Elastomer base and trichloro(1H,1H,2H,2H-perfluorooctyl) silane were purchased from Sigma-Aldrich (St. Louis, MO, USA). Poly (lactic-*co*-glycolic) acid-polyethylene glycol copolymer was purchased from PolySciTech (Akina, West Lafayette, IN, USA). Cholesterol (CHO) and 1,1′-dioctadecyl-3,3,3′,3′-tetramethylindocarbocyanine perchlorate (DiI) were purchased from Sigma-Aldrich (St. Louis, MO, USA). 1,2-Dimyristoyl-sn-glycero-3-phosphocholine (DMPC), cholesterol and 1,2-distearoyl-sn-glycero-3-phosphoethanolamine-N-[amino(polyethylene glycol)-2000] (DSPE) were obtained from Nanocs (New York, NY, USA).

3. Experimental methods

3.1. Hydrogel preparation

Collagen gel was prepared following the manufacturer's instructions. Corning High Concentration Rat Tail collagen, Type 1 was diluted to the desired concentration using deionised water (dI) and 10× phosphate buffered saline (PBS). 1.0 M sodium hydroxide (NaOH) solution was

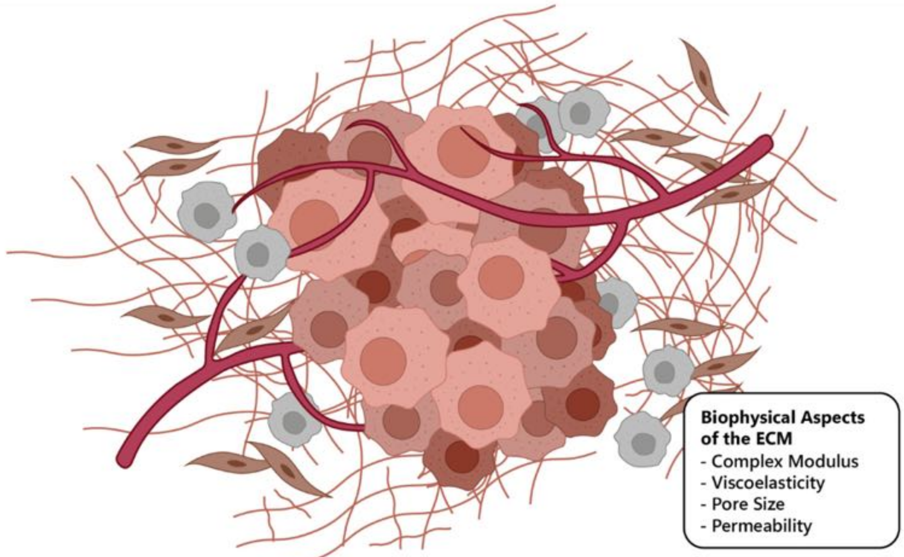

Fig. 1. Tumor microenvironment consisting of tumor cells, tumor associated fibroblast and immune cells and ECM. Biophysical properties of the ECM include complex modulus, viscoelasticity, pore size and diffusive permeability of molecules or particles.

used to adjust pH to 7. The temperature of all components was maintained at 4 °C during the preparation process to prevent gelation. The prepared collagen solution was then pipetted and gelated by incubation at 37 °C, 5% CO_2 and constant humidity for 1 h before use.

Matrigel was prepared using a Corning® Matrigel® matrix stock solution according to the manufacturer's protocol. Briefly, Matrigel® (kept at −20 °C) was thawed on ice overnight before use. Matrigel was then diluted to desired concentrations using ice-cold 1× PBS. Then the Matrigel solution was mixed by pipetting up and down and vortexing gently. As the polymerisation of Matrigel is temperature dependent, it is important to carry out all the steps at 4 °C. The solution was then pipetted into the defined geometry, and gelated by incubating at 37 °C, 5% CO_2 and constant humidity for 1 h before use.

Low melting point (LMP) agarose was diluted with water to produce the intended concentrations and was placed in a snap-cap vial to prevent evaporation during the heating process. The mixture was heated to 75 °C and kept at this temperature for 15 min, while being vortexed every 3 min. The solution was then pipetted into the intended geometry and set at room temperature for 15 min before being set at 4 °C in a refrigerator for 1 h.

3.2. *Rheometry*

Oscillatory rheometry was conducted to characterize the viscoelastic properties of each hydrogel (over a range of concentrations) using a TA Instruments ARG-G2 Rheometer (New Castle, DE). Collagen gel and Matrigel were prepared following Manufacturer's protocol and left to gelate within an incubator at 37 °C. Low Melting Point Agarose was left to gelate at 24 °C for 60 min (gel forms <30 °C), before being placed into a 37 °C incubator an hour for rheometer testing. The testing geometry used was an 8 mm parallel plate, following an existing protocol for the rheological characterization of hydrogels as an initial guide [20]. The test geometry was lowered to 300 μm above the rheometer plate, and then the testing sequence was applied to each sample at 37 °C (Table 1). The testing sequence includes a conditioning step, a strain sweep, then a frequency sweep followed by a time sweep. Each sample underwent the initial conditioning step; however, a fresh sample was required for each strain sweep; frequency sweep; and time sweep, due to hydrogel viscoplasticity. Agarose gel, an almost purely elastic polymer gel, found a plateau at a lower strain and higher frequency. Matrix viscoplasticity means each testing sequence produces long-term irreversible deformation of the matrix, so multiple tests cannot be performed on one sample. The strain (%) and frequency (rad/s) values reported for each sample in Table 1 are within the linear viscoelastic range. Each sample was only characterized once, with 3–5 independent samples being characterized and averaged for each gel concentration.

The reported storage modulus (G′) and complex modulus (G*) for each gel at each concentration were taken from the time sweep data set, and the complex modulus calculated using Eq. 1. The loss tangent (or tan δ), a measure of the ratio of viscous (energy dissipation) to elastic (energy storage) response of a viscoelastic material when under load, was used for simplicity as a single parameter comparator of the viscoelasticity of each hydrogel and calculated using Eq. 2 from the values of G′ and G″ taken from the time sweep data (Figs. S3–S5).

Table 1
Rheometry parameter table.

Hydrogel	Parameter	Strain sweep (% strain)	Frequency sweep (rad/s)	Time sweep (5 min)
Agarose gel	Temperature (°C)	37	37	37
	Frequency (rad/s)	50	0.01–100	5
	% strain	0.1–100	0.1	0.1
Collagen gel	Temperature (°C)	37	37	37
	Frequency (rad/s)	50	0.01–100	1
	% strain	0.1–100	1	1
Matrigel	Temperature (°C)	37	37	37
	Frequency (rad/s)	50	0.1–100	1
	% strain	0.01–100	10	10

$$\mathrm{G}^{*} = \sqrt{\text{Storage Modulus } (\mathrm{G//})^{2} + \text{Loss Modulus } (\mathrm{G}')^{2}} \tag{1}$$

$$tan\delta = \frac{\text{Loss Modulus } (\mathrm{G}')}{\text{Storage Modulus } (\mathrm{G}'')} \tag{2}$$

3.3. *Cell culture*

Skov3 cells were cultured in DMEM supplemented with 10% fetal bovine serum, 100 U/mL penicillin, and 100 U/mL streptomycin (GIBCO, USA). Each flask was incubated at 37 °C, 5% CO_2 and constant humidity. Cells were trypsinized and passaged after reaching 70–80% confluence. Skov3 cells were selected as a model cell line which responds to the mechanical property of the ECM microenvironment [21]. To produce spheroid laden Matrigel, Skov3 tumor spheroids were cultured using liquid overlay techniques [22]. Skov3 cells were seeded at a density of 5×10^3 cells/well into a 96-well plate, which was precoated with 50 μL of 2% agarose gel. The formation of the spheroids was then initiated by centrifugation (1000g, 10 min). Cells were cultured for additional 7 days within the same incubator before use. After 7 days the spheroids were mixed with Matrigel and incubated for a further 3 days to allow ECM remodeling.

3.4. *Critical point drying*

A Tousimis AUTOSAMADRI-815 Critical Point Drier (CPD) was used to dry hydrogel samples so they could be imaged with a conventional high vacuum Scanning Electron Microscope (SEM). Prior to critical point drying, hydrogel samples were excised to known dimensions by scalpel or tissue punch and placed wet (under DI water) into specimen pots of 12.5 mm in diameter with porous lids (CPD800A Proscitech, Australia) for dehydration. Samples were progressively dehydrated at RT using in a series of ethanol solutions of 60, 90, and 100 wt% (minimum 3 h per step), with a final overnight 100% ethanol step. The samples (8 samples max) immersed in 100 wt% ethanol were then placed into the CPD chamber and cooled to an operational temperature of −10 °C. The chamber was then flooded with liquid CO_2 and the samples were run through a purge cycle for 45 min, held in statis mode for 1 h, purged again for 45 min and held for a final hour in a statis mode before complete drying of the sample. The statis mode was used to remove the liquid CO_2 and leave the samples completely dry.

3.5. *Scanning Electron Microscopy (SEM)*

After drying, the dimensions of the samples were measured using a light microscope to determine a CPD sample shrinkage factor. Dried samples were stored in a vacuum desiccator until required for Scanning Electron Microscopy (SEM). For SEM, samples were attached by sticky carbon tabs to SEM pin-stubs, Plasma cleaned with an Evactron 25 plasma cleaner for 10 min, then sputter coated with Pt to a thickness of 10–15 nm. These samples were then imaged using a SU3500 Hitachi SEM or JEOL 7100F SEM at 100× to 60,000× magnification. Images were then uploaded to Adobe Photoshop and converted from RGB to Grayscale format. The image contrast and brightness were maximized, to show the largest variation between fiber and the space surrounding them.

3.6. Pore size analysis using a MATLAB program

The MATLAB program was developed to estimate the largest circle that fits within the Critical Point Dried (CPD) fibers and the standard deviation (necessary for heterogeneous hydrogels). The program is new, as it allows for the accurate automated analysis of hydrogel pore size and fiber size. The program, initially, takes the greyscale image and binarizes it using thresholding. This thresholding requires the initial analysis of the contrast and light within each hydrogel structure, and it differs dependent on magnification. The image was then be median filtered, and a Euclidean distance transformation was performed. The Euclidean distanced plot was then smoothed using a Gaussian (Gaussian kernel = 5) and disk filter (disk kernel = 5). The coordinates of the maximum distance (the radius to the closest fibers) were then identified and scaled up based on the sample shrinkage. The pore sizes were averaged for each image using 8–12 images per sample for 2–3 samples of the same hydrogel.

3.7. Synthesis of nanoparticles

Liposome and poly(lactic-*co*-glycolic acid) (PLGA) nanoparticles were synthesized using a one-step microfluidic method [23]. Briefly, 1,2-dimyristoyl-sn-glycero-3-phosphocholine (DMPC), cholesterol and 1,2-distearoyl-sn-glycero-3-phosphoethanolamine-N-[amino(polyethylene glycol)-2000] (DSPE) were dissolved in chloroform. The chloroform was then removed from the solution using a rotary evaporator, producing a lipid film. A solution of anhydrous isopropyl alcohol (IPA) with DiI dye was added to dissolve the lipid film. Then a flow focusing microfluidic device was used to create liposomes by flowing the lipid solution through the central stream while PBS was perfused into the side streams. The liposomes were stored in a 4 °C fridge for further use.

PLGA nanoparticles were also synthesized using a one-step microfluidic method. PLGA-PEG copolymer and fluorescent dye DiI were dissolved in acetonitrile [24]. This solution was then flowed through the central stream of the microfluidic device and squeezed by MilliQ water that was introduced from the two side channels. All NPs prepared in the microfluidic device were purified by dialysis using a cellulose membrane with a size of 10 kDa and immersed in PBS. Particle size was measured using Dynamic Light Scattering (DLS) and Transmission Electron Microscopy (TEM).

3.8. Microfluidic device fabrication

Microfluidic devices were fabricated using a standard photolithography and soft lithography techniques [25]. AutoCAD was used to produce the pattern and printed onto a chrome mask. SU-8 dry film was used to coat silicon wafers and baked, followed by UV exposure through the mask. After postbaking the wafers were developed and washed, removing excess SU-8. The wafer was salinized with trichloro (1H,1H,2H,2H-perfluorooctyl) silane as a protective coating. To produce the PDMS microfluidic devices Sylgard 184 Silicone Elastomer curing agent and Sylgard 184 Silicone Elastomer base were degassed and allowed to polymerize at 80 °C on the wafer. The crosslinked PDMS was then peeled off the wafer, hole punched and cut into single devices. These devices and their glass slides were then oxygen plasma coated and adhered together to produce the microfluidic device.

3.9. Measurement of hydrogel diffusive permeability coefficient

To measure particle diffusive permeability coefficient (P_d) in hydrogels, fluorescent nanoparticles were utilized. P_d measures the flux of a molecule (of known molecular weight/size) across a porous barrier. A Zeiss Confocal Microscope was used to gather fluorescent intensity images (10× magnification) over time within the Regions of Interests (ROI). The five regions of interest were drawn using the Zen software within the hydrogel, after the trapezoidal pillars. A 543-nm-wavelength laser was used to excite the diI (1,1′-dioctadecyl-3,3,3′,3′-tetramethylindocarbocyanine perchlorate (‘DiI’; $DiIC_{18}(3)$)) fluorescence, and measurements were recorded every 2 s for a total of 2–5 min. The correlation between fluorescent intensity, within each ROI, over time was then normalized and approximated by a line of best-fit. The slope of this line is represented as $dI_{avg,\ gel}/dt$ in Eq. 3, and the P_d is calculated using the following equation,

$$P_{app} = \frac{A_{ROI}\left(\frac{dI_{avg,gel}}{dt}\right)}{w_{pillars}\left(I_{capillary} - I_{lymph}\right)_{t=0}} \tag{3}$$

where A_{ROI} is the average area of the ROI. $w_{pillars}$ represents the width of the area through which the articles are permeating from the channel into the hydrogel, and $I_{capillary}$ is the initial fluorescent intensity when the channel is filled with nanoparticles. I_{lymph} is defined as the initial fluorescent intensity within the lymph channel with no nanoparticles present. The difference between $I_{capillary}$ and I_{lymph} is normalized against the fluorescent intensity for each test. All particle transport was driven by diffusion.

3.10. Statistical analysis

To measure *p*-values and standard deviation, data was input into IBM SPSS Statistics used a two-tailed analysis. A Bivariate Correlation test was performed based on the Pearson model, to flag significant correlations of the raw data. Significant correlations were denoted by ***, **, * represent statistically significant difference ($p < 0.001$, $p < 0.05$, and $p < 0.01$). Within this test a standard deviation of each data set was calculated.

4. Results and discussion

4.1. Hydrogel rheometry

The rheological properties of the ECM play very important roles in regulating tumor growth and invasion [26–28]. The storage modulus and loss modulus of the three hydrogels were measured (Fig. 2) and then converted to the complex modulus (G*) and tan δ, as a comparative measure of viscoelasticity. The storage modulus is an indication of the hydrogels' resistance to deformation (elasticity). The loss modulus represents the energy dissipated (viscosity). The complex modulus (Eq. 1) considers the sum of the storage (recoverable deformation) and loss modulus (non-recoverable deformation), representing the overall resistance to deformation of a gel. The viscoelasticity of a material can be represented in many ways, but in this work, we use tan δ, which is calculated from the ratio of the loss modulus to the storage modulus, with δ ranging from 0° (for a purely elastic response) to 90° (for a purely viscous response) [29]. It has been reported that changes in ECM viscoelasticity has been associated with cancer progression [30,31].

The complex modulus G* is calculated as an indication of the overall gel stiffness. All the three hydrogels have complex moduli dominated by the storage moduli, and they exhibited the expected positive correlation between protein concentration and complex modulus [20,32]. The Collagen gel has a complex modulus of 20–70 Pa over 1.5–6.7 mg/mL protein concentrations (1 Rad/s, 1% strain) (Fig. 2a), aligning with those literature reports of G* from 2.2–17 Pa, at 1 rad/s, 2% strain, for lower collagen gel concentrations (0.4–2.0 mg/mL) [33]. At a frequency of 1–6.3 rad/s, Holder et al. reported a complex modulus of 20 Pa for 4 mg/mL collagen gel [29]. Agarose gels at the concentrations of 1–3 wt% have complex moduli of 9000–50,000 Pa at 5 rad/s and 0.1% strain (Fig. 2b). Deepthi et al. reported a smaller G* of 800–4000 Pa for 0.5–0.8%wt. at 1 rad/s agarose gel [34] and at 0.1–10 rad/s. Balgude et al. reports a G* of 100–1300 Pa (1–2 wt% agarose gel) [35]. Matrigel presents a complex modulus of 60–400 Pa, for protein concentrations of 5.7–10.8 mg/mL (Fig. 2c). Semler et al. described a complex modulus of

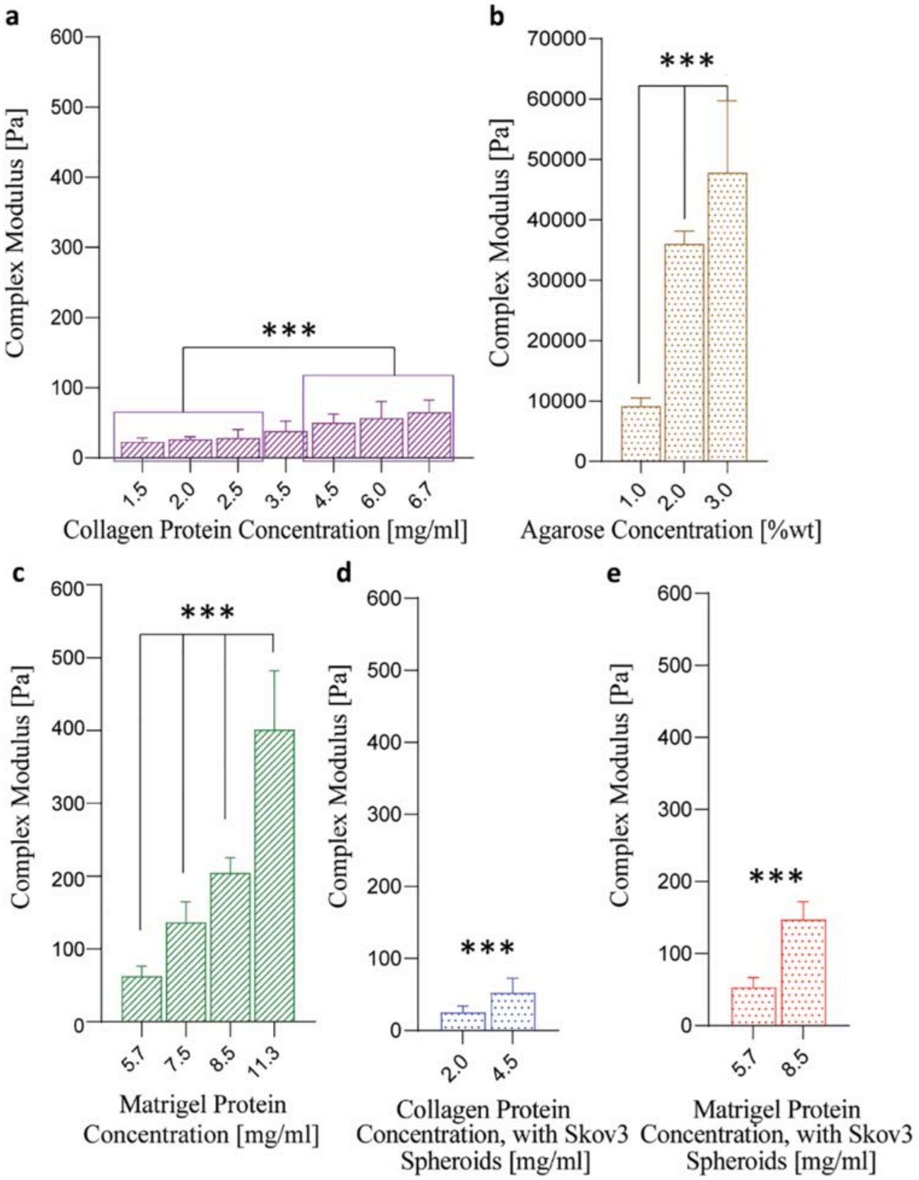

Fig. 2. Complex moduli (G*) of a) collagen gel (1 rad/s, 1% strain), b) Agarose gel (5 rad/s, 0.1% strain), c) Matrigel (1 rad/s, 10% strain), d) Skov3 laden collagen gel (1 rad/s, 1% strain), and e), Skov3 laden Matrigel (1 rad/s, 10% strain), cultured for 24 h. ***, **, and * represent statistically significant difference ($p < 0.001$, $p < 0.05$, and $p < 0.01$).

~34 Pa at 1 rad/s for a 100% Matrigel solution [36], and Slater et al. reported a complex modulus of 10–100 Pa for 3–9 mg/mL Matrigel concentrations at 3.2 rad/s and 0.25 strain. These literature results correlate well with what we measured in this work.

Skov3 spheroid laden Matrigel and collagen gels were included to investigate the effect of the loaded spheroids in hydrogel on their biophysical properties. Within *in vivo* conditions, the presence of tumor cells and other stroma cells stiffens the matrix, but on the other hand collagen gel and Matrigel could be degraded over time [1,37,38]. The spheroid laden Matrigel was cultured for 24 h and the complex moduli were measured to analyze whether degradation or stiffening of the matrix occurred. Compared to the complex moduli of Matrigel (60–400 Pa), the spheroid laden Matrigel's (5.7–8.5 mg/mL) exhibited similar complex moduli (50–150 Pa) (Fig. 2d). Spheroid laden collagen gel also illustrated a similar complex modulus (25 and 53 Pa) to the same collagen gel concentration without spheroid addition (26 and 50 Pa). These findings indicate that the incorporation of spheroids (with a 24-hour culture time) has limited impact on the complex modulus of the hydrogel. This is probably due to the lack of stromal cells as well as the small size and number of spheroids incorporated in our experiments, as within *in vivo* conditions the cellular components (*e.g.* tumor cells and stroma cells) contribute 80% to the total volume of tumor tissues [39–41].

Based on our experimental results, it is not straightforward to directly compare the hydrogel complex moduli (~20–400 Pa for collagen gel and Matrigel) we measured in this study to those *in vivo* ECM results, as literatures only reports the overall tissue complex modulus which consists of ECM and cellular components in the tissue. Therefore, we need to remove the contributions of cells to isolate the ECM modulus. This can be estimated by assuming, as reported in literature, that 80% or less of the tumor tissue by volume is cellular (within breast cancer) [41]. Then we can assume that the ECM equals to 20% of the complex modulus of tumor tissue (~5–1000 Pa) [42]. This means an estimation of a complex moduli range between 1 and 600 Pa could be assumed for an *in vivo* ECM, under the assumption that 1.) all cells and ECM are separable contributions to mechanical properties; and 2.) the contribution of cells to the overall mechanical property of tissue samples is similar to that of the ECM. As a result, the estimated 1–600 Pa exhibits a greater stiffness range, but correlates well with the moduli of collagen gel and Matrigel of low concentrations characterized this study [43].

Viscoelastic materials display time-dependent strain or stress responses to deformation [29,31]. At the same frequency and strain, the lower the value of the loss tangent, the lower the relative value of the viscous or dissipative response of a material is compared to the elastic response, *i.e.* the less viscoelastic a material is. In this study, we use Tan δ to represent the quantitative viscoelasticity property of hydrogels. Tan δ values of collagen (1 rad/s), Matrigel (1 rad/s), and agarose gels (5 rad/s) were measured over a range of concentrations (Fig. 3a–e). Collagen gel exhibited the highest tan δ, ranging from 0.19 to 0.25 at the protein concentrations of 2.0–6.7 mg/mL. The tan δ remained constant at ~0.2 for those collagen gels with concentrations over 2.0 mg/mL. Fig. 3f depicts the tan δ as a function of δ angle for collagen gel with different concentrations. Spheroid laden collagen gels (Fig. 3e) at the concentrations of 2.0 and 4.5 mg/mL, exhibit similar tan δ (0.21 and 0.25, respectively) as those collagen gels without spheroids (Fig. 3a). The collagen gel had the highest tan δ of all the hydrogels, as illustrated by the δ angle (Fig. 3f and j) both with and without spheroid incorporation. In comparison, Matrigel showed relatively lower tan δ of 0.1–0.2 at the protein concentrations of 5.7–8.5 mg/mL for the gels with and without spheroids (Fig. 3b and d). As illustrated in Fig. 3g and i, the tan δ for both Matrigel with and without spheroids was close to purely elastic. The tan δ of agarose gels (1–3 wt%) spanned 0.03–0.11 (Fig. 3c), representing an almost purely elastic polymer gel (Fig. 3h). This matches the literature reported range of tan δ of 0.01–0.2 for 2–4% agarose gels, over a frequency range 1–125 rad/s [44]. Moreover, each hydrogel demonstrated an inverse relationship between their tan δ and protein concentration.

We next compared the tan δ results of the three gels in this study with those in literature. Rheological analysis of lung ECM presented a loss tangent (measured *via* AFM at 7.2 rad/s [45]) of 0.06, and infarcted heart ECM (mice) had a loss tangent ranging from 0.1–0.25 (AFM measurements at 0.35 and 72 rad/s [46]), which are similar to the range exhibited by all the different gels in our study (except 1.5 and 2.0 mg/mL collagen gel). This indicates that collagen gel, Matrigel and 1 wt% agarose concentration display similar ranges of loss tangent matching the bounds of soft tissue with *in vivo* relevance, while higher concentrations of agarose gel fall outside of the bounds.

4.2. Pore size of hydrogels

The pore sizes of the three hydrogels were determined using a new method which combines SEM imaging and a MATLAB image processing program. Gelated samples were dried using the Critical Point Drying (CPD) method [47], leaving only the fibrous "skeleton" for imaging [48]. The sample shrinkage was factored into pore size calculations. Then the platinum coated "skeleton" was imaged under a SEM. 8–12 images were taken for each sample at different magnifications. Fig. 4A1, B1 and C1 show the SEM images of 2 mg/mL collagen gel (10× magnification), 4 mg/mL Matrigel® (5× magnification) and 2 wt% agarose gel (60× magnification), respectively. These images were post-processed using Photoshop (Fig. 4A2, B2 and C2), and then analyzed using a MATLAB program which approximates circles of the largest diameters between fibers (Fig. 4A3, B3 and C3), representing the pores within the sample. Our MATLAB method was carefully validated using literature images and their estimated pore size (Fig. S1). Reporting similar pore sizes (using MATLAB processing) to those presented in literature (using low resolution images) for collagen and agarose gel [49–55]. Compared to those previously reported methods which often manually assess pore sizes in SEM images, our automated MATLAB technique allows much more accurate, quicker and reliable measurement of pore size.

The morphologies of the three hydrogels are distinct. Collagen gel shows fine fibers similar to those reported in literature, which can be visualized using a confocal [53,56] and SEM microscope [57,58]. Matrigel has a fibrous and sheet structure which are visible under SEM [59–63]. Agarose gel has a thicker fibrous and nodular structure, which is only visible under a SEM microscope at high magnifications [48,64,65]. Agarose gel (1–3 wt%) exhibits the smallest pore size, ranging from 120 to 270 nm, while collagen gel (1.5–6.7 mg/mL) has a slightly larger pore size between 690 and 1350 nm (Fig. 5.a). Matrigel has the largest pore size ranging from 570 to 2520 nm, within the SEM

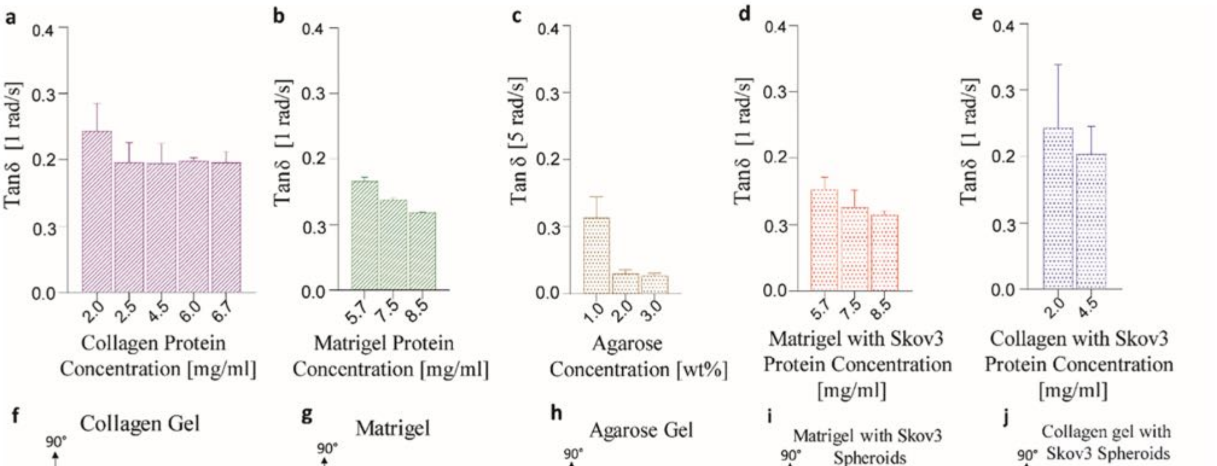

Fig. 3. Tan δ of different hydrogels. a) Collagen gel, b) Matrigel, c) agarose gel, d) Matrigel with Skov3 spheroids and e) collagen gel with Skov3 spheroids (cultured for 24 h), along with the representation of tan δ as an angle between 0° (a purely elastic response) and 90° (a purely viscous response) for graphs f) collagen gel, g) Matrigel, h) agarose gel, including i) Matrigel and j) collagen gel with Skov3 spheroids. δ is presented as it's angular representation. δ in this presentation shows how most of the viscoelasticity of the gels are closer to the purely elastic δ than the purely viscous δ.

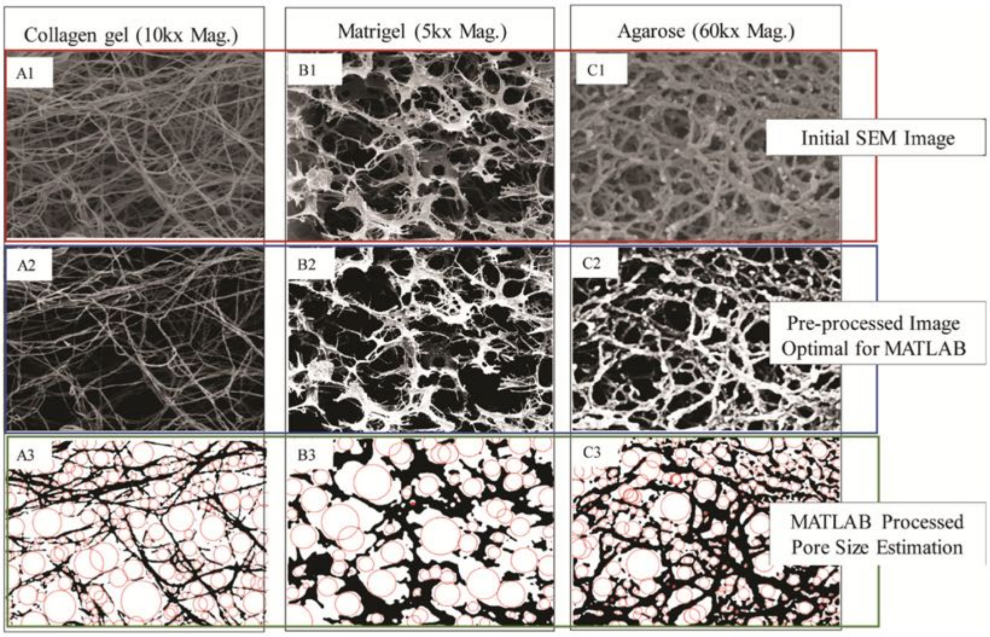

Fig. 4. SEM images of gels and image processing for pore size analysis. A) 2 mg/mL Collagen, B) 4 mg/mL Matrigel and C) 2 wt% agarose.

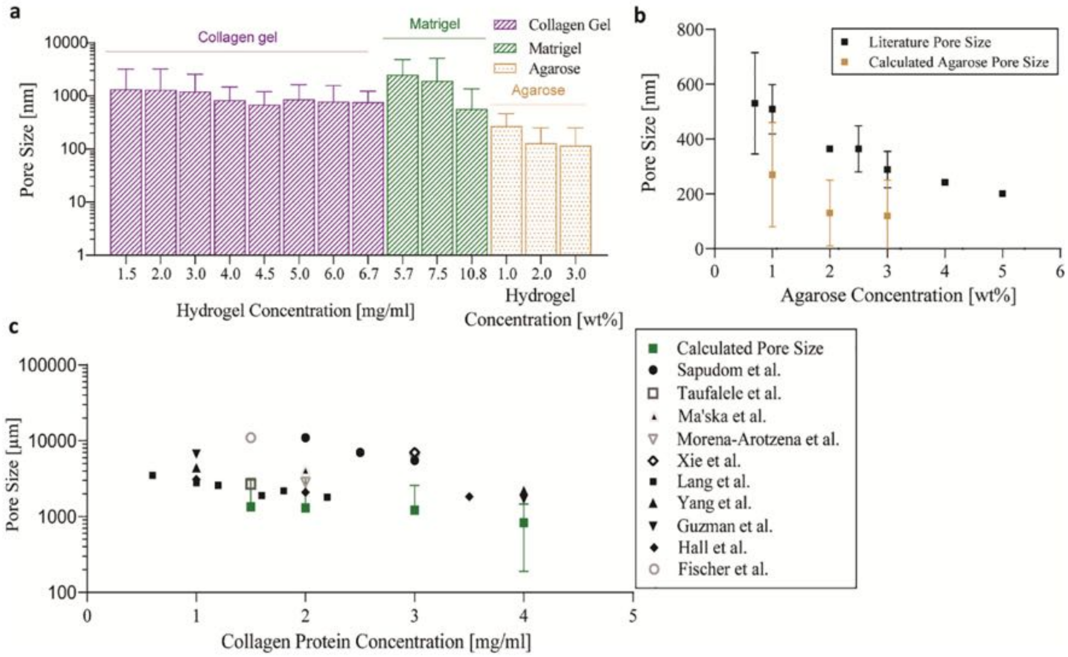

Fig. 5. Pore sizes of hydrogels with different protein concentrations. a) Measured pore size of Matrigel, collagen gel and agarose gel. b) Comparison of the pore size of agarose gel between our measurement and those reported in literature [67–70]. c) Pore sizes of collagen reported in literature [49,51–53,56,58,71–74] in comparison to our measured pore sizes.

images as indicated by its sheet and fibrous structure, this morphology produced a large variability in pore size measurement due to batch to batch variation. As expected, across all gels the pore size has an inverse relationship to protein/polymer concentration [66].

Compared to those measured by Atomic Force Microscopy (AFM) [69,70], the pore sizes we measured for Agarose ranged from 120 to 270 nm in diameter, similar to those reported by Mounir et al. (200–530 nm) (Fig. 5b). The pore sizes reported in literature for collagen gel (1500–11,000 nm) from 0.6–4 mg/ml were just above the bounds of our measured pore size of 690–1350 nm for comparative concentrations (Fig. 5c). Our method produces an average pore size slightly smaller than those reported previously which could be mainly due to the limited resolution of Confocal images and limited sample size, the limitations of manual measurement using SEM image manual analysis [49,51–53,56,58,71,73–75], while it should be noted that *in vivo* ECM has much smaller pore sizes ranging from 3 to 500 nm [66].

As Matrigel has a combination of sheet and fiber structure, it is difficult to ascertain its pore size due to the varying pore size between different morphologies [59–63]. Also, the ratio of sheet to fiber structure changes with Matrigel concentration and purchase batch, a common challenge for characterizing a naturally derived (extracellular matrix mouse sarcoma) matrix. Nevertheless, our measured pore size of

570–2520 nm, an average of fiber and sheet pore size, aligns with the approximation of 2000 nm for (~5–6 mg/ml Matrigel) reported by Zaman et al [76].

When it comes to analysing the pore size of hydrogels, a consensus about the best approach has yet to be achieved [66]. A particle permeation method has been attempted to quantify the maximum particle size which permeates through a hydrogel matrix. This method is limited by possible hydrogel-particle charge interaction and particle size variability resulting in significantly reduced accuracy. Alternatively, it is more straightforward to analyze microscopic images of a gel morphology and estimate the pore size. Confocal microscope images have been used extensively. However, with limited magnification the spaces between the hydrogel matrix fibers (at 37 °C) are often invisible, limiting its capability in pore analysis [49,51–53,56,71,73–75]. Recent studies have focused on the analysis of SEM images obtained using CryoSEM or CPD drying techniques (removing or solidifying water). CryoSEM freezes the hydrogel at -200 °C and the matrix is imaged while maintaining the freezing conditions within the SEM chamber. However, artefacts in CryoSEM are difficult to avoid as water within the sample crystalizes and expands the matrix.

The CPD technique we used in this study removes all water content from the sample and is often utilized for imaging fine features (fibers). Dried "skeleton" of the hydrogel can be imaged under typical SEM (room temperature) conditions, and the pore size is approximated. Existing techniques mainly use manual analysis, where a few pore diameters are manually measured for several images and averaged, which is prone to human error and does not fully describe the heterogeneity of a hydrogel. We created an automated MATLAB pore finding program in conjunction with CPD drying [73] to accurately measure the pore size of hydrogels. Our method can improve the accuracy of hydrogel pore size measurement. This is critical as the pore size acts as a key regulator of mechanical confinement, which affects cell phenotype and migration [31].

4.3. Diffusive permeability coefficient of hydrogels using a microfluidic device

Hydrogel diffusive permeability is a crucial biophysical factor when fabricating an *in vitro* cancer model as it affects nutrient availability and removal, and therapeutic drug extravasation. In most *in vivo* conditions, the ECM presents minimal impedance to drug delivery in contrast to the cellular monolayers (endothelium). However, targeted therapies rely on a leaky endothelium (the so-called enhanced permeability and retention effect, EPR) to allow drug-laden particles (~100 nm) to enter the ECM [77]. Therefore, the fibrous ECM to some extent presents a barrier to therapeutic delivery [77]. By quantifying the diffusive permeability coefficient (P_d), the flux of a molecule across a barrier, we can determine the speed at what drugs are able to reach target cells within the matrix [69,78]. The P_d is the diffusive component, without convective flow, that drives solute permeability [79]. P_d, within this research, is also considered a relative permeability measurement [80,81].

Initial relative permeability testing was conducted using 20 kDa dextran (6.9 nm in diameter by DLS), which can easily permeate the ECM [82], and 70 kDa dextran (10.6 nm in diameter by DLS) mimicking macromolecules like albumin (68 kDa), the most abundant protein in blood which are relatively impermeable to blood vessels [83]. Dextran is a neutrally charged particle that has been extensively used in medical research [84]. Also, the relative permeability of two nanoparticles (NPs), liposome and poly(lactic-*co*-glycolic acid) (PLGA) NPs was also determined for mimicking nanomedicines [85]. These two particles namely PLGA (114 nm, −10 mV) and liposome (98.7 nm, −18 mV) have similar particle size and charge [86]. The slightly negative charge of the nanoparticles is favorable for drug delivery, as it prevents nonspecific interactions between nanoparticles and the biological environment.

To measure the diffusive permeability coefficient (P_d) of each hydrogel, a three-channel microfluidic device was designed (Fig. 6b) with the side channels to introduce fluid flow, and the middle channel to confine a hydrogel (Fig. S2). The trapezoid-shaped pillars are able to trap the hydrogel in the middle channel by surface tension. A fluorescent particle-laden solution was introduced to the "capillary" channel, and particles permeated through the hydrogel to the "lymph" channel. Using a Confocal Microscope, Regions of Interest (ROI's) of the fluorescence within the hydrogel could be tracked over time to calculate P_d [68]. The ROI layout in Fig. S2 is necessary for input into the P_d calculations, and normalization of the fluorescent fluctuations within the middle hydrogel channel over time. The temperature (37 °C), pH (7) and dilution medium (PBS) were kept constant during the studies.

The diffusive permeability coefficient of the selected NPs was measured in collagen gel with protein concentrations of 1.5–6.7 mg/mL (Fig. 6a). As expected, the P_d of all the nanoparticles, regardless of their sizes, exhibited an inverse relationship with the hydrogel protein concentration, which agrees with literature results [51,71,75]. High protein concentrations correlate to a smaller pore size [87,88]. As the diffusion time (T_D) of a molecule has an inverse correlation with particle size, the increase of particle size leads to a longer diffusion time, thus decreased diffusive permeability [89,90].

At the same protein concentration (2.2 mg/mL), 70 kDa dextran had a significantly ($p < 0.05$) smaller diffusive permeability coefficient (2570 nm/s) than 20 kDa (3140 nm/s) in collagen, suggesting a direct negative correlation between P_d and particle size. This negative correlation is also valid for larger nanoparticles. 70 kDa dextran has a diffusive permeability coefficient 4-fold greater than liposome NPs (460–640 nm/s) and 20-fold greater than the PLGA NPs (40–110 nm/s). Interestingly, the soft liposome NPs (460–640 nm/s) exhibits several-fold greater permeability than the rigid PLGA NPs (40–110 nm/s). Tomasetti et al. also observed an even greater 10-fold increase in P_d of soft liposomes compared to hard PLGA NPs [88]. The enhanced permeability of soft NPs is mainly due to their flexible structures and deformability. Yu et al. demonstrated using molecular dynamics (MD) simulations and super-resolution microscopy that semi-elastic spherical NPs deformed into ellipsoids within hydrogel mesh structures, inducing rotation-facilitated fast diffusion [91]. Latreille et al. also reported a spontaneous shrinking of soft NPs in confined hydrogel environments resulting in faster diffusion compared to hard non-deformable particles [92].

The diffusive permeability coefficient in Matrigel was measured over a range of protein concentrations (5.7–10.8 mg/mL) (Fig. 6a). Within

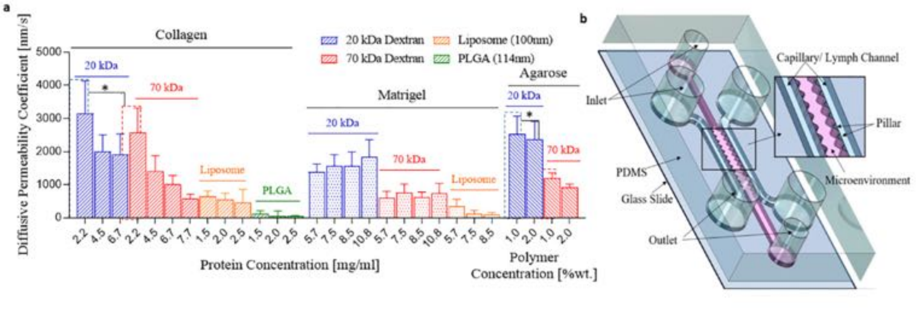

Fig. 6. The relative a) diffusive permeability coefficient (P_d) of different molecules and nanoparticles in hydrogels, including 20 kDa (~7 nm in diameter) and 70 kDa (~11 nm in diameter) dextran, liposome nanoparticles (~100 nm in diameter) and PLGA nanoparticles (~114 nm in diameter). ***, **, * represent statistically significant difference ($p < 0.001$, $p < 0.05$, and $p < 0.01$). b) Schematic of a three-channel microfluidic device designed to measure hydrogel permeability, consisting of two liquid channels (outer channels) and loading of hydrogels in the middle channel.

Matrigel, 20 kDa dextran exhibited a greater P_d than 70 kDa dextran. Specifically, 20 kDa dextran displayed a significantly greater ($p < 0.05$) P_d of 1830 nm/s than that of the 70 kDa dextran (750 nm/s) in 10.8 mg/mL Matrigel. 70 kDa dextran had a 2-fold greater P_d than the larger (100 nm) liposome NPs (100–350 nm/s). Like collagen, particle P_d's in Matrigel also exhibits a direct negative relationship with particle size.

The P_d values of 20 kDa and 70 kDa dextran in agarose gel were measured at concentrations of 1 and 2 wt% (Fig. 6a), showing a similar trend that the diffusive permeability coefficient decreases with the increase of agarose concentration and particle size, similar to those described in literature [69,70]. The P_d of 20 kDa dextran (2520 nm/s) in 1 wt% agarose gel is 2-fold greater than 70 kDa dextran (1190 nm/s) ($p < 0.001$) (Fig. 6a). The P_d of liposomes and PLGA nanoparticles in agarose was too small to be determined.

Comparing the three hydrogels (collagen, Matrigel and agarose), the agarose gel has a similar dextran P_d to collagen gel, but slightly greater than Matrigel, despite its much smaller pore sizes (190–410 nm). The P_d values of dextran and liposome in Matrigel (100–1380 nm/s) were less than that in collagen gel (460–3140 nm/s), despite Matrigel having a larger pore size (2300–2900 nm) than the collagen gel (700–1500 nm). This could be due to the sheet-fiber morphology of Matrigel, small particles being trapped in large spaces with Brownian motion creating a longer path length thus decreased P_d. Electrostatic interactions might also play some roles as all particles and Matrigel are negatively charged [88,93]. The P_d's of dextran and NPs studied in this work have important implications for nanoparticle drug delivery. It is apparent that the smaller the particle, the more effectively it permeates the ECM [94]. For both collagen gel and agarose gel, the P_d decreased with the increased concentration of gels.

In contrast, P_d within *in vivo* tissue is far slower than pure ECM, as it is comprised of 80% cells by volume (within breast cancer) which represents a significant diffusion barrier [39–41]. To estimate the isolated impact of the ECM on Pd, Ho et al. reported the Pd of 70 kDa dextran through fibrin gel with Human Umbilical Vein Endothelial Cells (HUVECs) ranged between 50 and 250 nm/s [80], which was an order of magnitude greater than Lee et al.'s uses the same P_d equation to calculate a "permeability coefficient" of 16 nm/s using the exact same model [95]. Polacheck et al. also reported a P_d of 60 nm/s with only endothelial cells with 70 kDa dextran into collagen I gel, and 180 nm/s with 10 kDa dextran [81]. A very similar device to this research was used by Zervantonakis et al. to measure the diffusive permeability coefficient of an endothelial monolayer channel into type I collagen gel, with a P_d of 400 nm/s with 10 kDa dextran, and 70 nm/s with 70 kDa [96]. The P_d of an endothelial layer into Matrigel, was 1.6–16 nm/s, dependent on the endothelial cell type, with 70 kDa dextran [97]. With the literature reporting P_d ranging from 16 to 400 nm/s when an endothelium is incorporated, in contrast to our 40–3140 nm/s in a hydrogel, the endothelium clearly impedes P_d 70–80%.

In vivo models of the microvasculature demonstrated an even more pronounced decrease in diffusive solute permeability. The vascular permeability, based of diffusivity of a molecule captured through fluorescent intensity within a region of interest, of liposome nanoparticles in tumor tissues is around 0.2 nm/s, which is much lower than that of albumin (the size of 70 kDa dextran) at 1.2 nm/s [98]. A similar study reported a vascular permeability, driven by diffusion, of 0.1 nm/s for liposomes and 6.6 nm/s for albumin in tumor tissue [99]. Yuan et al. also measured the solute permeability of 70 kDa dextran within cerebral microvessels at 1.5 nm/s [100]. In general, the reported diffusive solute permeability of *in vivo* tissue is 92–99% slower than that within an ECM mimicking hydrogel.

4.4. Correlation between hydrogel biophysical properties

With the complex modulus, loss tangent, pore size and permeability (P_d) measured, the interdependence between them was also explored. The P_d of the 20 kDa dextran is independent of tan δ, complex modulus, and pore size because of its extremely small size. For the other three particles with bigger sizes (70 kDa dextran, liposome and PLGA), the P_d shows a somewhat direct correlation with tan δ though with a limited number of data points (Fig. 7a) [31], whereas an inverse relationship exists between P_d and the complex modulus (Fig. 7b), except the 70 kDa dextran in Matrigel. These trends are expected, as an increase in viscoelastic behavior should produce a decrease in matrix connectivity, allowing more space for particle permeation. A direct relationship also exists between pore size and complex modulus (Fig. 7c), and tan δ (Fig. 7d). Within agarose gel these associations can be described using network theory, where increased gel concentration induces more crosslinking [101,102]. Collagen gel appears to follow a similar premise, although the matrix does not "crosslink". This increased crosslinking, decreases the loss tangent (less potential for energy dissipation compared to higher potential for energy storage) and pore size, which decreases P_d due to smaller distances between network junctions. Increased network junctions mean an increase in complex modulus. As a result, the biophysical properties of collagen gel and agarose gel can by altered by gel concentration. An aspect outside the scope of this study is that when gel concentration increases, the scaffold density is increased and the biochemical potential of the ECM changes due to increased ligand availability.

Matrigel, however, indicated no relationship between its biophysical properties, proving a difficult matrix to quantify, which agrees with literature reports [103,104]. Collagen gel and agarose gel are natural polymers, whereas Matrigel is a derived tumor ECM (mouse sarcoma extracellular matrix proteins and basement membrane proteins) and is a mixture of many components [105].

5. Conclusions

This work systematically investigated the biophysical characteristics of ECM-mimicking hydrogels (Matrigel, collagen gel, agarose gel), including complex modulus, loss tangent, pore size and diffusive permeability. The complex moduli of Matrigel with (50–430 Pa) and without (60–400 Pa) Skov3 spheroid addition and collagen gel with (25 and 53 Pa) and without (26 and 50 Pa) Skov3 spheroid addition, fall within the estimated range of *in vivo* cancer tissue ECM (~1–600 Pa). The tan δ of Matrigel with and without Skov3 (0.1–0.2) and collagen gel with and without Skov3 spheroid addition (0.2–0.25) correlates well with those *in vivo* reconstituted ECM and soft tissue (0.1–0.2) [31,106], but agarose gel fell outside of this range with a tan δ of 0.03–0.11. Altering collagen and agarose gel concentration illustrated a positive correlation with complex modulus, and an inverse correlation with the loss tangent; these associations can be explained by network theory [101]. The biophysical properties of collagen gel and agarose gel present as a function of gel concentration, and thereby altering protein or polymer concentration can be used to tune the gel's biophysical characteristics [107,108].

We developed a new combined approach of CPD, SEM imaging and MATLAB processing for the quantification of hydrogel pore size. Only agarose gel (120–270 nm) produced a pore size within the *in vivo* ECM range (3–500 nm), whereas Matrigel (570–2520 nm) and collagen gel (690–1350 nm) had much larger pore sizes mainly due to the lack of cellular components. collagen gel, agarose gel and Matrigel did demonstrate the expected direct relationship between pore size and protein concentration, making it possible to tune the gel pore size for tumor models using protein concentration [66].

ECM diffusion driven permeability was quantified using a microfluidic-based method. As expected, particle diffusion has an inverse relationship with particle size. Interestingly, the stiffness of nanoparticles significantly affects their diffusive permeability through the matrix. Soft liposome particle (460–640 nm/s) exhibited a far greater diffusion driven matrix permeability then the stiffer PLGA NP (40–110 nm/s). Nanoparticles have comparable diffusive permeability coefficients in collagen gel (40–3140 nm/s) and agarose gel (750–2520

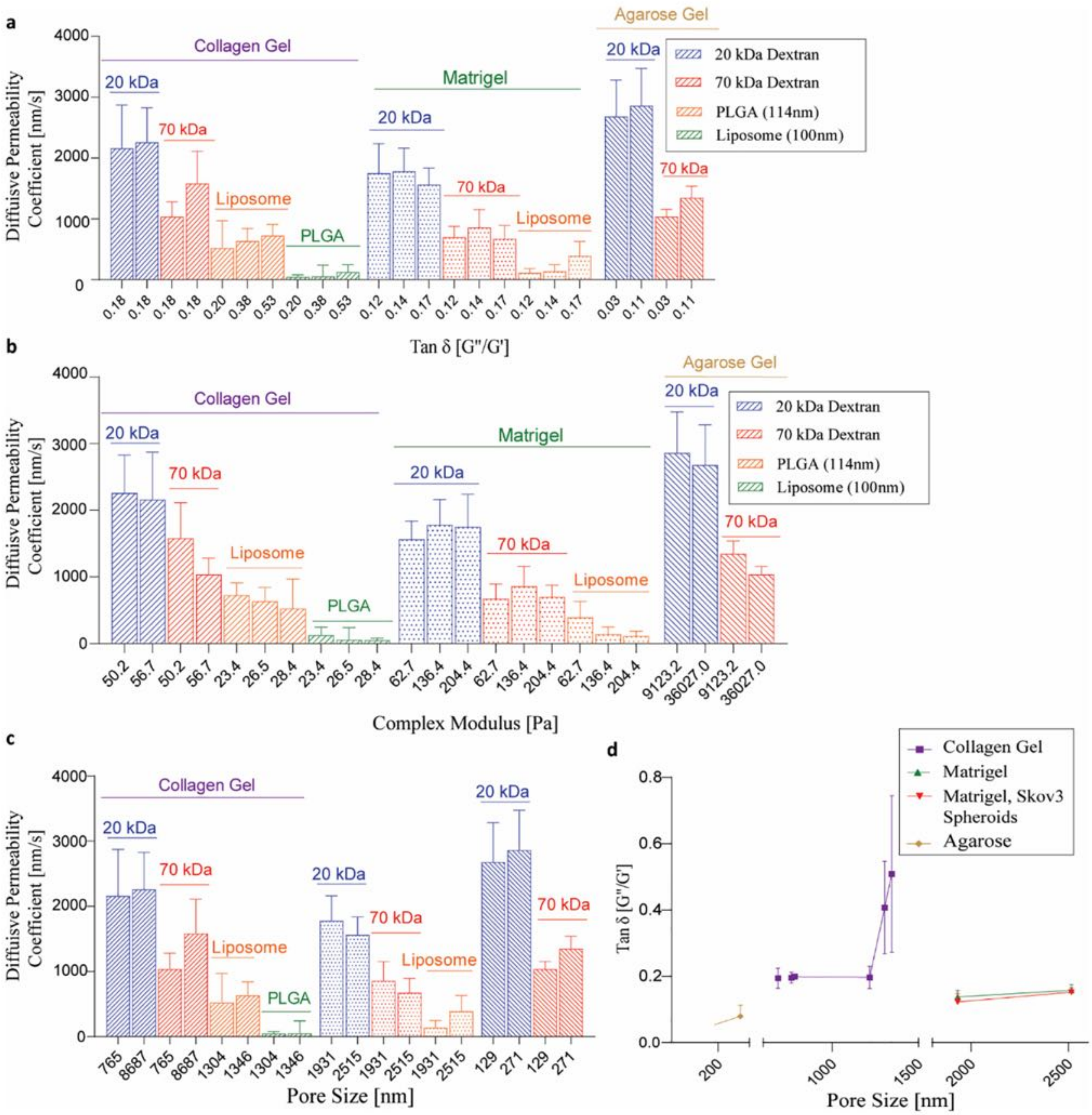

Fig. 7. Diffusive permeability coefficients of 20 kDa (~7 nm in diameter), 70 kDa (~11 nm in diameter), liposome NPs (~100 nm in diameter) and PLGA NPs (~114 nm in diameter) with respect to a) viscoelasticity, tan δ; b) storage modulus; c) pore size. d) Correlation between pore size and viscoelasticity (tan δ).

nm/s) dependent upon the protein or polymer concentration. In contrast, they exhibited the lowest P_d in Matrigel (100–1380 nm/s) and showed no dependence on protein concentration. Matrigel (the ECM of a mouse sarcoma) thus, appeared to not exhibit any correlations between range of measured biophysical properties and architectural characteristics and proved a difficult matrix to quantify. Collagen gel and agarose gel showed a direct proportionality between protein/biopolymer concentration and complex modulus, and an inverse relationship between protein/biopolymer concentration and pore size. In summary, the biophysical properties of hydrogels and their interdependence are intricate, and the new approaches developed, the systematic studies conducted, and the data presented in this study will provide useful information for selecting suitable hydrogel materials for mimicking *in vivo* extracellular matrix.

Funding sources

This research was supported by the Australian Research Council projects (FT140100726 and DP200101238).

CRediT authorship contribution statement

Anna P. Cameron: Methodology, Writing – original draft, Writing – review & editing, Software, Validation, Formal analysis, Investigation. **Bijun Zeng:** Investigation. **Yun Liu:** Investigation. **Haofei Wang:** Investigation. **Farhad Soheilmoghaddam:** Investigation. **Justin Cooper-White:** Methodology, Writing – review & editing, Investigation, Formal analysis. **Chun-Xia Zhao:** Conceptualization, Methodology, Writing – original draft, Writing – review & editing, Supervision, Project administration, Funding acquisition.

Declaration of competing interest

The authors declare no conflict of interest.

Acknowledgment

This research was supported by the Australian Research Council projects (FT140100726 and DP200101238). This work was performed in part at the Queensland node of the Australian National Fabrication Facility, a company established under the National Collaborative Research Infra-Structure Strategy to provide nano- and microfabrication facilities for Australia's researchers. The authors also acknowledge the facilities, and the scientific and technical assistance from Kim Sewell, at the Australian Microscopy & Microanalysis Research Facility, the Centre for Microscopy and Microanalysis, The University of Queensland.

References

[1] Y. Li, E. Kumacheva, Hydrogel microenvironments for cancer spheroid growth and drug screening, Sci. Adv. 4 (2018), eaas8998.

[2] V. Poltavets, M. Kochetkova, S.M. Pitson, M.S. Samuel, Front. Oncol. 8 (2018) 431.

[3] C. Walker, E. Mojares, A.Del Rio Hernandez, Int. J. Mol. Sci. 19 (2018).

[4] R. Kalluri, R.A. Weinberg, J. Clin. Invest. 119 (2009) 1420–1428.

[5] C. Frantz, K.M. Stewart, V.M. Weaver, J. Cell Sci. 123 (2010) 4195–4200.

[6] M. Zanoni, F. Piccinini, C. Arienti, A. Zamagni, S. Santi, R. Polico, A. Bevilacqua, A. Tesei, Sci. Rep. 6 (2016) 19103.

[7] H.-F. Tsai, A. Trubelja, A.Q. Shen, G. Bao, J. R. Soc. Interface (2017), https://doi.org/10.1098/rsif.2017.0137.

[8] Q. Chai, Y. Jiao, X. Yu, Gels (2017) 3.

[9] H.H.G. Song, K.M. Park, S. Gerecht, Journal (2014), https://doi.org/10.1016/j.addr.2014.06.002.

[10] K. Talkenberger, E.A. Cavalcanti-Adam, A. Voss-Bohme, A. Deutsch, Sci. Rep. 7 (2017) 9237.

[11] A.F. Barendsz-Janson, A.D. Muller, H.H.C. Lichtenbelda, M.C.E van Dam-Mieras, H.F.P Hillen, Tumor Biol. 19 (1998) 104–112.

[12] S.S. Kumar, The International Young Researchers' Conference, 2021, https://doi.org/10.34614/iyrc0056.

[13] G. Fang, H. Lu, A. Law, D. Gallego-Ortega, D. Jin, G. Lin, Lab Chip 19 (2019) 4093–4103.

[14] S. Berzina, A. Harrison, V. Taly, W. Xiao, Cancers (Basel) 13 (2021).

[15] J. Kulwatno, J. Gearhart, X. Gong, N. Herzog, M. Getzin, M. Skobe, K.L. Mills, Integr. Biol. (Camb.) 13 (2021) 1–16.

[16] G. Cheng, J. Tse, R.K. Jain, L.L. Munn, PLoS One 4 (2009), e4632.

[17] A.C.N.Annika M. Bourgonje, Jan T.G. Schepens, Kiek Verrijp, Liesbeth Hovestad, Riet Hilhorst, Sheila Harroch, Pieter Wesseling, William P.J. Leenders, Wiljan J.A. J. Hendriks, Oncotarget 5 (2014) 8690–8702.

[18] M. Swamydas, J.M. Eddy, K.J. Burg, D. Dreau, In Vitro Cell. Dev. Biol. Anim. 46 (2010) 673–684.

[19] X. Gong, J. Kulwatno, K.L. Mills, Acta Biomater. (2019), https://doi.org/10.1101/815662.

[20] J.M. Zuidema, C.J. Rivet, R.J. Gilbert, F.A. Morrison, J. Biomed. Mater. Res. B Appl. Biomater. 102 (2014) 1063–1073.

[21] A.J. McKenzie, S.R. Hicks, K.V. Svec, H. Naughton, Z.L. Edmunds, A.K. Howe, Sci. Rep. 8 (2018) 7228.

[22] A. Boussommier-Calleja, R. Li, M.B. Chen, S.C. Wong, R.D. Kamm, TrendsCancer 2 (2016) 6–19.

[23] R. Ran, H.F. Wang, F. Hou, Y. Liu, Y. Hui, N. Petrovsky, F. Zhang, C.X. Zhao, Adv. Healthc. Mater. 8 (2019), e1900015.

[24] Y. Liu, Y. Hui, R. Ran, G.Z. Yang, D. Wibowo, H.F. Wang, A.P.J. Middelberg, C. X. Zhao, Adv. Healthc. Mater. 7 (2018), e1800106.

[25] D.C.D.J.Cooper MacDonald, Janelle R. Anderson, Daniel T. Chiu, Hongkai Wu, Olver J.A. Schueller, George M. Whitesides, Electrophoresis 21 (2000) 27–40.

[26] D.M. Gilkes, G.L. Semenza, D. Wirtz, Nat. Rev. Cancer 14 (2014) 430–439.

[27] E.M. Grasset, T. Bertero, A. Bozec, J. Friard, I. Bourget, S. Pisano, M. Lecacheur, M. Maiel, C. Bailleux, A. Emelyanov, M. Ilie, P. Hofman, G. Meneguzzi, C. Duranton, D.V. Bulavin, C. Gaggioli, Cancer Res. 78 (2018) 5229–5242.

[28] Q. Yu, Y. Xue, J. Liu, Z. Xi, Z. Li, Y. Liu, Front. Mol. Neurosci. 11 (2018) 130.

[29] A.J. Holder, N. Badiei, K. Hawkins, C. Wright, P.R. Williams, D.J. Curtis, Soft Matter 14 (2018) 574–580.

[30] A.N. Ketene, E.M. Schmelz, P.C. Roberts, M. Agah, Nanomedicine 8 (2012) 93–102.

[31] O. Chaudhuri, J. Cooper-White, P.A. Janmey, D.J. Mooney, V.B. Shenoy, Nature 584 (2020) 535–546.

[32] C.A. Grattoni, H.H. Al-Sharji, C. Yang, A.H. Muggeridge, R.W. Zimmerman, J. Colloid Interface Sci. 240 (2001) 601–607.

[33] R.K. Willits, S.L. Skornia, J. Biomater. Sci. Polym. Ed. 15 (2004) 1521–1531.

[34] R.B.R. Deepthi, K. Jagadeesh, M.S. Vijaya, SASTECH J. 9 (2010) 27–30.

[35] X.Y.A.P. Balgude, A. Szymanski, R.V. Bellamkonda, Biomaterials 22 (2001) 1077–1084.

[36] C.S.R.Eric J. Semler, Prabhas V. Moghe, Biotechnol. Bioeng. 69 (2000) 359–369.

[37] K.M. Park, D. Lewis, S. Gerecht, Annu. Rev. Biomed. Eng. 19 (2017) 109–133.

[38] J.L. Leight, A.P. Drain, V.M. Weaver, Annu.Rev.Cancer Biol. 1 (2017) 313–334.

[39] A. Naba, K.R. Clauser, S. Hoersch, H. Liu, S.A. Carr, R.O. Hynes, Mol. Cell. Proteomics 11 (M111) (2012), 014647.

[40] T. Casey, J. Bond, S. Tighe, T. Hunter, L. Lintault, O. Patel, J. Eneman, A. Crocker, J. White, J. Tessitore, M. Stanley, S. Harlow, D. Weaver, H. Muss, K. Plaut, Breast Cancer Res. Treat. 114 (2009) 47–62.

[41] C. Ianniello, L. Moy, J. Fogarty, F. Schnabel, S. Adams, D. Axelrod, L. Axel, R. Brown, G. Madelin, Sci. Rep. 11 (2021) 5156.

[42] J.R. Staunton, W. Vieira, K.L. Fung, R. Lake, A. Devine, K. Tanner, Cell. Mol. Bioeng. 9 (2016) 398–417.

[43] A. Nabavizadeh, M. Bayat, V. Kumar, A. Gregory, J. Webb, A. Alizad, M. Fatemi, Sci. Rep. 9 (2019) 5737.

[44] Q. Chen, B. Suki, K.N. An, J. Biomech. Eng. 126 (2004) 666–671.

[45] T. Luque, E. Melo, E. Garreta, J. Cortiella, J. Nichols, R. Farre, D. Navajas, Acta Biomater. 9 (2013) 6852–6859.

[46] I. Andreu, T. Luque, A. Sancho, B. Pelacho, O. Iglesias-Garcia, E. Melo, R. Farre, F. Prosper, M.R. Elizalde, D. Navajas, Acta Biomater. 10 (2014) 3235–3242.

[47] A. Sinha, A. Guha, Mater. Sci. Eng. C 29 (2009) 1330–1333.

[48] M.C. Nweke, M. Turmaine, R.G. McCartney, D.G. Bracewell, Biotechnol. J. (2017) 12.

[49] N.R. Lang, S. Munster, C. Metzner, P. Krauss, S. Schurmann, J. Lange, K. E. Aifantis, O. Friedrich, B. Fabry, Biophys. J. 105 (2013) 1967–1975.

[50] D.A. Bell, C. Santeufemio, Microsc. Microanal. 12 (2006) 1124–1125.

[51] A. Guzman, M.J. Ziperstein, L.J. Kaufman, Biomaterials 35 (2014) 6954–6963.

[52] M.S. Hall, F. Alisafaei, E. Ban, X. Feng, C.Y. Hui, V.B. Shenoy, M. Wu, Proc. Natl. Acad. Sci. U. S. A. 113 (2016) 14043–14048.

[53] P.V. Taufalele, J.A. VanderBurgh, A. Munoz, M.R. Zanotelli, C.A. Reinhart-King, PLoS One 14 (2019), e0216537.

[54] M.J. Moore, F. Bodera, C. Hernandez, N. Shirazi, E. Abenojar, A.A. Exner, M. C. Kolios, Nanoscale 12 (2020) 21420–21428.

[55] H.M.J.Rodriguez Corral, M. Zhang, P. Maiello, Can. Geotech. J. 57 (2020) 12.

[56] J. Xie, M. Bao, S.M.C. Bruekers, W.T.S. Huck, ACS Appl. Mater. Interfaces 9 (2017) 19630–19637.

[57] S.P. Reese, N. Farhang, R. Poulson, G. Parkman, J.A. Weiss, Biophys. J. 111 (2016) 1797–1804.

[58] O. Moreno-Arotzena, J.G. Meier, C. Del Amo, J.M. Garcia-Aznar, Materials (Basel) 8 (2015) 1636–1651.

[59] Y.S. Zhang, Y.N. Zhang, W. Zhang, Drug Discov. Today 22 (2017) 1392–1399.

[60] W. Asghar, H. Shafiee, P. Chen, S. Tasoglu, S. Guven, U.A. Gurkan, U. Demirci, in: Cancer Targeted Drug Delivery, 2013, pp. 635–665, https://doi.org/10.1007/978-1-4614-7876-8_24, ch. Chapter 24.

[61] E.A. Neofytou, E. Chang, B. Patlola, L.M. Joubert, J. Rajadas, S.S. Gambhir, Z. Cheng, R.C. Robbins, R.E. Beygui, J. Biomed. Mater. Res. A 98 (2011) 383–393.

[62] H.J. Kim, D.X. Oh, S. Choy, H.-L. Nguyen, H.J. Cha, D.S. Hwang, Cellulose 25 (2018) 7299–7314.

[63] A.L. Placone, P.M. McGuiggan, D.E. Bergles, H. Guerrero-Cazares, A. Quinones-Hinojosa, P.C. Searson, Biomaterials 42 (2015) 134–143.

[64] A. Salerno, R. Borzacchiello, P.A. Netti, J. Appl. Polym. Sci. 122 (2011) 3651–3660.

[65] C.E.E.Xingdong Wang, Meifang Zhou, Kathryn Prince, David R.G. Mitchell, Rachel A. Caruso, Chem. Comm. 29 (2007) 3060–3062.

[66] L. Tomasetti, M. Breunig, Adv. Healthc. Mater. (2018) 7.

[67] N. Pernodet, M. Maaloum, B. Tinland, Electrophoresis 18 (1997) 55–58.

[68] J. Narayanan, J.-Y. Xiong, X.-Y. Liu, J. Phys. Conf. Ser. 28 (2006) 83–86.

[69] M. Maaloum, N. Pernodet, B. Tinland, Electrophoresis 19 (1998) 1606–1610.

[70] K.C. Labropoulos, S. Rangarajan, D.E. Niesz, S.C. Danforth, J. Am. Ceram. Soc. 84 (2001) 1217–1224.

[71] J. Sapudom, S. Rubner, S. Martin, T. Kurth, S. Riedel, C.T. Mierke, T. Pompe, Biomaterials 52 (2015) 367–375.

[72] R.C. Arevalo, J.S. Urbach, D.L. Blair, Biophys. J. 99 (2010) L65–L67.

[73] T. Fischer, A. Hayn, C.T. Mierke, Sci. Rep. 9 (2019) 8352.

[74] C. E. Martin Maška, Javier Fernández-Marqués, Arrate Muñoz-Barrutia, Michal Kozubek, and Carlos Ortiz-de-Solórzano, 2015.

[75] Y.L. Yang, S. Motte, L.J. Kaufman, Biomaterials 31 (2010) 5678–5688.

[76] L. M. T. Muhammad H. Zaman, Alisha L. Sieminski, Drew MacKellar, Haiyan Gong, Roger D. Kamm, Alan Wells, Douglas A. Lauffenburger, and Paul Matsudaira, 2005.

[77] H.F. Wang, R. Ran, Y. Liu, Y. Hui, B. Zeng, D. Chen, D.A. Weitz, C.X. Zhao, ACS Nano 12 (2018) 11600–11609.

[78] R. Richter, M.A.M. Kamal, M.A. Garcia-Rivera, J. Kaspar, M. Junk, W.A. M. Elgaher, S.K. Srikakulam, A. Gress, A. Beckmann, A. Grissmer, C. Meier, M. Vielhaber, O. Kalinina, A.K.H. Hirsch, R.W. Hartmann, M. Bronstrup, N. Schneider-Daum, C.M. Lehr, Mater. Today Bio 8 (2020), 100084.

[79] N.T. Elliott, F. Yuan, J. Pharm. Sci. 100 (2011) 59–74.

[80] Y.T. Ho, G. Adriani, S. Beyer, P.-T. Nhan, R.D. Kamm, J.C.Y. Kah, Sci. Rep. 7 (2017), 707.

[81] W.J. Polacheck, M.L. Kutys, J.B. Tefft, C.S. Chen, Nat. Protoc. 14 (2019) 1425–1454.

[82] B. Neu, R. Wenby, H.J. Meiselman, Biophys. J. 95 (2008) 3059–3065.

[83] A. Hoffmann, J. Bredno, M. Wendland, N. Derugin, P. Ohara, M. Wintermark, Transl. Stroke Res. 2 (2011) 106–111.

[84] I. Wasiak, A. Kulikowska, M. Janczewska, M. Michalak, I.A. Cymerman, A. Nagalski, P. Kallinger, W.W. Szymanski, T. Ciach, PLoS One 11 (2016), e0146237.

[85] M.E. Davis, Z.G. Chen, D.M. Shin, Nat. Rev. Drug Discov. 7 (2008) 771–782.

[86] R. Ran, A.P.J. Middelberg, C.X. Zhao, Colloids Surf. B: Biointerfaces (2016), https://doi.org/10.1016/j.colsurfb.2016.09.016.
[87] M.L. Oyen, Int. Mater. Rev. 59 (2013) 44–59.
[88] L. Tomasetti, R. Liebl, D.S. Wastl, M. Breunig, Eur. J. Pharm. Biopharm. 108 (2016) 145–155.
[89] B. Amsden, Polymer Gels And Networks, 1996.
[90] D. de Beer, Biotechnol. Bioeng. 53 (1997) 151–158.
[91] M.R. Yu, L. Xu, F.L. Tian, Q. Su, N. Zheng, Y.W. Yang, J.L. Wang, A.H. Wang, C. L. Zhu, S.Y. Guo, X.X. Zhang, Y. Gan, X.F. Shi, H.J. Gao, Nat. Commun. (2018) 9.
[92] P.L. Latreille, V. Adibnia, A. Nour, J.M. Rabanel, A. Lalloz, J. Arlt, W.C.K. Poon, P. Hildgen, V.A. Martinez, X. Banquyf, Nat. Commun. (2019) 10.
[93] J.M. Newby, I. Seim, M. Lysy, Y. Ling, J. Huckaby, S.K. Lai, M.G. Forest, Adv. Drug Deliv. Rev. 124 (2018) 64–81.
[94] S. Barua, S. Mitragotri, Nano Today 9 (2014) 223–243.
[95] H. Lee, S. Kim, M. Chung, J.H. Kim, N.L. Jeon, Microvasc. Res. 91 (2014) 90–98.
[96] I.K. Zervantonakis, S.K. Hughes-Alford, J.L. Charest, J.S. Condeelis, F.B. Gertler, R.D. Kamm, Proc. Natl. Acad. Sci. U. S. A. 109 (2012) 13515–13520.
[97] G. Li, M.J. Simon, L.M. Cancel, Z.D. Shi, X. Ji, J.M. Tarbell, B. Morrison 3rd, B. M. Fu, Ann. Biomed. Eng. 38 (2010) 2499–2511.
[98] F. Yuan, M. Leunig, S.K. Huang, D.A. Berk, D Papahadjopoulos, R.K. Jain, Cancer Res. 54 (1994) 3352–3356.
[99] C.B. Rygh, S. Qin, J.W. Seo, L.M. Mahakian, H. Zhang, R. Adamson, J.Q. Chen, A. D. Borowsky, R.D. Cardiff, R.K. Reed, F.R. Curry, K.W. Ferrara, Clin. Cancer Res. 17 (2011) 550–559.
[100] W. Yuan, Y. Lv, M. Zeng, B.M. Fu, Microvasc. Res. 77 (2009) 166–173.
[101] E.M. Grad, I. Tunn, D. Voerman, A.S. de Leon, R. Hammink, K.G. Blank, Front. Chem. 8 (2020) 536.
[102] S. Hayashi, Polym. J. 10 (1978) 59–67.
[103] E. Polykandriotis, A. Arkudas, R.E. Horch, U. Kneser, Am. J. Pathol. 172 (2008) 1441, author reply 1441–1442.
[104] E.A. Aisenbrey, W.L. Murphy, Nat. Rev. Mater. 5 (2020) 539–551.
[105] L. S. Corning Incorporated, 2018.
[106] O. Chaudhuri, L. Gu, D. Klumpers, M. Darnell, S.A. Bencherif, J.C. Weaver, N. Huebsch, H.P. Lee, E. Lippens, G.N. Duda, D.J. Mooney, Nat. Mater. 15 (2016) 326–334.
[107] M. Cavo, M. Fato, L. Penuela, F. Beltrame, R. Raiteri, S. Scaglione, Sci. Rep. 6 (2016) 35367.
[108] B. Trappmann, C.S. Chen, Curr. Opin. Biotechnol. 24 (2013) 948–953.